



Brazilian Journal of Physics

ISSN: 0103-9733

luizno.bjp@gmail.com

Sociedade Brasileira de Física  
Brasil

Foglio, M. E.; Barberis, G. E.  
Study of  $\text{Co}^{2+}$  in different crystal field environments  
Brazilian Journal of Physics, vol. 36, núm. 1A, march, 2006, pp. 40-54  
Sociedade Brasileira de Física  
São Paulo, Brasil

Available in: <http://www.redalyc.org/articulo.oa?id=46436109>

- How to cite
- Complete issue
- More information about this article
- Journal's homepage in redalyc.org

redalyc.org

Scientific Information System  
Network of Scientific Journals from Latin America, the Caribbean, Spain and Portugal  
Non-profit academic project, developed under the open access initiative

# Study of $\text{Co}^{2+}$ in Different Crystal Field Environments

M. E. Foglio and G. E. Barberis

Instituto de Física "Gleb Wataghin", UNICAMP, 13083-970, Campinas, São Paulo, Brazil

Received on 14 June, 2005; accepted on 28 November, 2005

We consider the ESR of  $\text{Co}^{2+}$  in different environments: in a regular octahedron ( $\text{Co}^{2+}$  in a MgO crystal), in a deformed octahedron ( $\text{Co}^{2+}$  in single crystals and powder samples of  $\text{NH}_4\text{NiPO}_4 \cdot 6\text{H}_2\text{O}$ ) or in a trigonal bipyramid ( $\text{Co}^{2+}$  in powders of  $\text{Co}_2(\text{OH})\text{PO}_4$  and  $\text{Co}_2(\text{OH})\text{AsO}_4$ ). We study the effect of the non-cubic crystal fields in the ESR of  $\text{Co}^{2+}$  in the deformed octahedron, by employing the normal modes of this structure to simplify the systematic study of the effect of these fields. A similar study was done for the deformed trigonal bipyramid, and it was necessary to derive the normal modes of this complex that are relevant to our problem.

Keywords: ESR; Crystal field

## I. INTRODUCTION

In the study of solid state systems, it is sometimes interesting to focus on the local states of the ions placed at the different sites of the crystal, either because they can be considered as the building blocks of the system, like in the tight binding method, or else because one is interested in the properties of a particular ion immersed in the solid, like in the study of the Electron Spin Resonance (ESR), or of the Raman scattering of impurities. We shall consider in particular the case of a ion  $\text{Co}^{2+}$  in different environments: in a regular octahedron ( $\text{Co}^{2+}$  in a MgO crystal[1]), in a deformed octahedron ( $\text{Co}^{2+}$  in single crystal and powder samples of  $\text{NH}_4\text{NiPO}_4 \cdot 6\text{H}_2\text{O}$ [2]) or in a trigonal bipyramid ( $\text{Co}^{2+}$  in powders of  $\text{Co}_2(\text{OH})\text{PO}_4$  and  $\text{Co}_2(\text{OH})\text{AsO}_4$ [3]).

The  $\text{Co}^{2+}$  in octahedral symmetry would be naively expected to suffer a static Jahn-Teller deformation, because the ground term  $^4F$  has a rather large orbital degeneracy, but instead it retains its cubic symmetry [1]. We shall briefly discuss the origin of this effect, and point out how the Jahn-Teller crystal fields affect the properties of the system. In a different symmetry, we shall use the normal modes of the octahedron formed by the nearest neighbors of  $\text{Co}^{2+}$  in  $\text{NH}_4\text{NiPO}_4 \cdot 6\text{H}_2\text{O}$  to study how the crystal fields affect the ESR of a single crystal of this compound. The  $\text{Co}^{2+}$  in a trigonal bipyramid surroundings appear in  $\text{Co}_2(\text{OH})\text{PO}_4$  and  $\text{Co}_2(\text{OH})\text{AsO}_4$ , and we have developed a study of the effect of crystal fields on its ESR that is similar to the one we employed for the deformation of the octahedron in  $\text{NH}_4\text{NiPO}_4 \cdot 6\text{H}_2\text{O}$ .

## II. THE $\text{Co}^{2+}$ IN A PERFECT OCTAHEDRAL SYMMETRY

In this section we shall consider a  $\text{Co}^{2+}$  ion in a perfect octahedral symmetry, as found when it is a substitutional impurity in crystalline MgO. This crystal has the NaCl structure, and the Co impurity is coordinated by six O ions in a regular octahedra. From any displacement of the six O with respect to the vertices of this regular octahedron we can find [4, 5] the corresponding normal coordinates  $Q_j$  of the seven ion complex, formed by the Co and the six nearest O, that are invariant against inversion. These are separated in the three

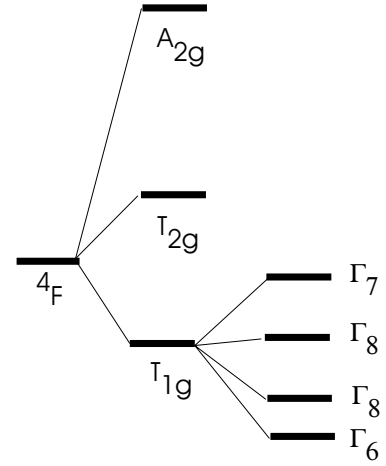


FIG. 1: Energy levels of the ground  $^4F$  term of a  $\text{Co}^{2+}$  split by a cubic field and by the spin orbit interaction. The levels are labelled by their symmetry properties.

sets  $\{Q_1\}$ ,  $\{Q_2, Q_3\}$  and  $\{Q_4, Q_5, Q_6\}$ , and the corresponding  $Q_j$  transform respectively like the basis of the irreducible representations  $A_1$ ,  $E$  and  $T_2$  of the cubic group, as given in Table II of reference 6.

The  $^4F$  ground state of isolated  $\text{Co}^{2+}$  ( $3d^7$ ) in a purely octahedral crystal field splits into two orbital triplets  $^4T_1$ ,  $^4T_2$  and one orbital singlet  $^4A_2$ , and from Jahn-Teller's theorem [7, 8] one would expect that the normal coordinates  $Q_j$  would take non-zero values to minimize the octahedron energy. This deformation does not occur, because the spin-orbit interaction stabilizes the average octahedral symmetry, by partially lifting the degeneracy of the  $^4T_1$  triplet into one  $\Gamma_6$ , two  $\Gamma_8$  and one  $\Gamma_7$  subspaces, as shown in figure 1.

We are mainly interested in the ESR of  $\text{Co}^{2+}$ , and the resonance for the lowest doublet ( $\Gamma_6$ ) is isotropic with  $g=4.33$  (cf. Sec. 7.14, p.447 in reference [9]). The addition of lower symmetry crystal fields produce further splittings of the  $^4T_1$  triplet, giving six Kramer's doublets, and in most cases it is found that the trace of the  $g$  tensor is close to the cubic isotropic value

[10].

In the lowest order one obtains  $g$  from the matrix elements of the Zeeman term in the  $\Gamma_6$  subspace of the  $^4T_1$  ground triplet. The matrix elements of the orbital angular momentum  $\mathbf{L}$  within a  $T_1$  subspace are proportional to those of a  $P$  term, but one should note that the excited term  $^4P$  is also of the  $^4T_1$  symmetry, and is mixed by the cubic field with the  $^4T_1$  of the ground  $^4F$  term. If we indicate two states of  $^4F$  and  $^4P$  with  $\phi_i$  and  $\phi'_i$  respectively, such that they transform in the same way under the cubic group, the states of the ground  $^4T_1$  will be of the form  $a\phi_i + b\phi'_i$ . The values of the constants  $a$  and  $b$  can be obtained [1, 11] from the Racah parameter  $B$  and the crystal field parameter  $Dq$ , that take the values  $815 \text{ cm}^{-1}$  and  $905 \text{ cm}^{-1}$  respectively for Co : MgO. With these values one obtains  $a = 0.9811$  and  $b = -0.1933$ , and the proportionality constant of the angular momentum is

$$\alpha = -1.5 a^2 + b^2 = -1.4063 \quad (1)$$

Two further effects should be considered in the calculation of the isotropic  $g$  tensor. One is the second order contribution of the  $^4T_2$  states, that are separated by  $\Delta'$  from the ground  $^4T_1$  states, and the other is the covalency between the Co and the neighboring O, described by several factors [1, 10], that reduce the matrix elements of the orbital angular momentum and of the spin orbit interaction. Using a single  $k_0$  for all these factors one obtains the expression for the  $g$  factor in a cubic field:

$$g = \frac{5}{3} g_e - \frac{2}{3} \alpha k_0 + 2 \left( \frac{\sqrt{15}}{2} a + b \right)^2 (k_0)^2 \frac{|\lambda|}{\Delta'} \quad (2)$$

where  $\lambda = -180 \text{ cm}^{-1}$  is the  $\text{Co}^{2+}$  spin-orbit interaction.

The expression given in reference [2] for  $\Delta'$  is not correct, and should be calculated as the difference between the level  $E(^4T_2)$  and the ground level  $E(^4T_1)$ . The ground  $E(^4T_1)$  level is the lowest eigenvalue of the matrix

$$\begin{vmatrix} -15B - 6Dq & 4Dq \\ 4Dq & 0 \end{vmatrix} \quad (3)$$

and the coefficients of the corresponding eigenvector give the  $a$  and  $b$  employed above to calculate the coefficient  $\alpha$  of the angular momentum.

The level  $^4T_2$  is given by

$$E(^4T_2) = -15B + 2Dq, \quad (4)$$

and in the present case, the choice of  $Dq = 905 \text{ cm}^{-1}$  and  $B = 815 \text{ cm}^{-1}$  gives  $E(^4T_2) - E(^4T_1) = \Delta' = 7953 \text{ cm}^{-1}$ . To adjust Eq. 2 to the experimental value it is then necessary to use  $k_0 = 0.86$ . In summary, the values for Co : MgO are  $a = 0.9811$ ,  $b = -0.1933$ ,  $\alpha = -1.4063$ ,  $\Delta' = 7953 \text{ cm}^{-1}$  and  $k_0 = 0.86$ . This last value seems too small, and one has to consider the dynamic Jahn-Teller effect [12, 13] to obtain a more reasonable value closer to 1.

To simplify the study we present a model that describes all the crystal fields acting on the Co as originating in the crystal field of the six nearest O located at the vertices of a deformed

octahedron, obtained by displacement of the vertices of the regular octahedron introduced at the beginning of this section. If one neglects the mixing of other configurations into the ground configuration  $(3d)^7$ , it is sufficient to keep only the part of the crystal field  $V$  that is even against inversion. We could then write  $V = \sum_{i=1}^7 V(\mathbf{r}_i)$ , where  $V(\mathbf{r})$  would be the sum of products of only two or four components of the electronic coordinates  $\mathbf{r}$ . Within our model, one could then write [4]

$$V(\mathbf{r}) = \sum_j Q_j V_j(\mathbf{r}) \quad (5)$$

where the  $Q_j$  and  $V_j(\mathbf{r})$  transform like the same partners of irreducible representations of the octahedral group [6]. As the  $V_j(\mathbf{r})$  must be even against inversion, the  $Q_j$  must have the same property, and only the six  $Q_j$  with  $j = 1, 6$  discussed at the beginning of this section would appear in Eq. (5). In the following we shall not consider the identical representation  $A_1$  because it does not modify the  $g$  tensor. The useful  $V_j(\mathbf{r})$  are then:

$$\begin{aligned} V_2(\mathbf{r}) &= A(x^2 - y^2) + B(x^4 - y^4) \\ \sqrt{3}V_3(\mathbf{r}) &= A(3z^2 - r^2) + B(2z^4 - x^4 - y^4) \end{aligned} \quad (6)$$

and

$$\begin{aligned} V_4(\mathbf{r}) &= Cxz + E(z^3y - y^3z) \\ V_5(\mathbf{r}) &= Cxz + E(x^3z - z^3x) \\ V_6(\mathbf{r}) &= Cxy + E(x^3y - y^3x) \end{aligned} \quad (7)$$

For a point charge model [4], the constants are given by

$$\begin{aligned} A &= \frac{1}{4} e e_{eff} (18R^{-4} - 75R^{-6}r^2), \quad B = 175 e e_{eff} / 8 R^6 \\ C &= e e_{eff} (-6R^{-4} + 15R^{-6}r^2), \quad E = -35 e e_{eff} / 2 R^6 \end{aligned} \quad (8)$$

where  $e_{eff}$  is an effective charge associated to the O.

The total Hamiltonian of the Co : MgO system can be written as

$$H_S = H_0 + H_{JT} = H_{S0} + H_v + H_{JT} \quad (9)$$

where  $H_v$  describes the vibrational states of MgO and  $H_{JT}$  the Jahn-Teller (JT) interaction, that we shall describe with Eq. (5). The eigenfunctions of the zeroth-order Hamiltonian  $H_0$  are products of the electronic functions  $\Gamma_6$ ,  $\Gamma_7$ ,  $\Gamma_8$ , and  $\Gamma'_8$ , times the vibrational functions of  $H_v$ . The normal coordinates of the seven ion complex in Eq. (5) are expressed in terms of the normal modes of the MgO or phonon variables [1], and this JT interaction mixes all these eigenstates of  $H_0$ : these linear combinations are the vibronic states of  $H_S$  which describe the states of the coupled system. The matrix elements related to the system properties are affected both by the structure of the vibronic states and by covalency, and the strength of the JT interaction can be related to measurements of the effect of applied stresses [11] on single crystals of MgO with  $\text{Co}^{2+}$  impurities. If one neglects the effect

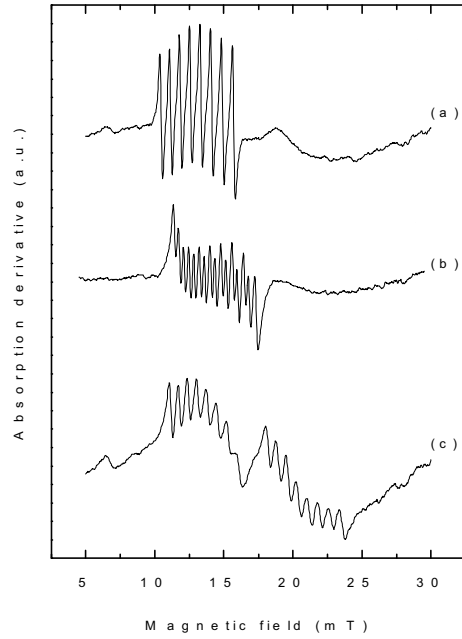


FIG. 2: Three  $\text{Co}^{2+}$  ESR spectra selected for directions of the magnetic field that show their properties as described in the text.

of covalency one obtains for the interaction constants  $V_j$  in Eq. (5) the values  $V_E \equiv V_2 = V_3 = 2.04 \cdot 10^{-11} \text{ cm}^{-1}/\text{cm}$  and  $V_T \equiv V_4 = V_5 = V_6 = 0.34 \cdot 10^{-11} \text{ cm}^{-1}/\text{cm}$ . Without entering into the details of the calculation [1] we can say that the experimental g factor  $g = 4.278$  [14] is explained by a JT coefficient  $V_E = 2.40 \cdot 10^{-11} \text{ cm}^{-1}/\text{cm}$  within the experimental error of 20% and a covalency factor  $k_0 = 0.96$ , much closer to one than the  $k_0 = 0.86$  derived in the absence of JT interaction. Employing an approximate phonon distribution [1], closer to the experimental one [15] than the single frequencies employed before [12, 13] to treat the JT interaction, it was also possible to describe the experimentally observed [16] Raman spectra of  $\text{Co} : \text{MgO}$  as the electronic Raman spectra of  $\text{Co}^{2+}$ .

We conclude that the JT effect is essential to understand the  $\text{Co}^{2+}$  ion in a perfect octahedral symmetry.

### III. THE $\text{Co}^{2+}$ IN A DEFORMED OCTAHEDRAL SYMMETRY

Figure 2 shows the ESR spectra of the single crystal sample measured at 4.2 K, for three selected directions of the magnetic field. The local symmetry of the nickel (II) ions is near cubic, and the Electron Spin Resonance (ESR) of impurity ions substituting Ni in the lattice is a powerful technique to analyze the environment of this ion. The ESR experiments make evident the difference between the two magnetically non-equivalent Ni sites that are present in the structure of  $\text{NH}_4\text{NiPO}_4 \cdot 6\text{H}_2\text{O}$ .

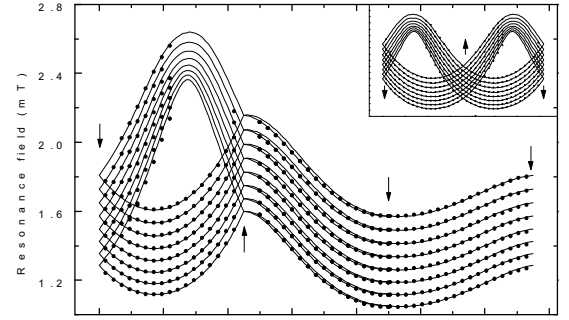


FIG. 3: Angular variation of spectra of  $\text{Co}^{2+}$  in  $\text{NH}_4\text{NiPO}_4 \cdot 6\text{H}_2\text{O}$ , in the three experimental planes. The principal directions in these planes are indicated in the figure. The solid lines are the best fit to the Eq. [10], and the fitting parameters are given in Table [I].

The spectra consist of two octets of resonance lines; those octets are due to the allowed transitions for  $\Delta S_z = \pm 1$ ,  $\Delta L_z = 0$  corresponding to the hyperfine interaction between the effective spin  $\vec{S} = 1/2$  of the cobalt and the real nuclear spin ( $I = 7/2$ ) of  $^{59}\text{Co}$  (100% abundant).

Figure 3 shows the angular variation of the resonance field of the ESR lines in the (100), (010) and (001) planes. Both the angular variation and its symmetry clearly show two magnetically nonequivalent sites related by a  $C_2$  operation about the c crystal axis, which is the point operation that relates the two centers. The actual spectra show eight well resolved hyperfine lines along some directions for each site; but the reduction of the hyperfine interaction causes the collapse of them in other directions (see Figure 2). The point group symmetry for the  $\text{Ni}^{2+}$  ion (and the  $\text{Co}^{2+}$  substituting them) is Cs, and the appropriate spin-Hamiltonian for  $\vec{S} = 1/2$  and  $\vec{I} = 7/2$  is therefore [9]:

$$\hat{H} = \mu_B \mathbf{H} \cdot \mathbf{g}_1 \cdot \mathbf{S}_1 + \mu_B \mathbf{H} \cdot \mathbf{g}_2 \cdot \mathbf{S}_2 + \mathbf{S}_1 \cdot \mathbf{A}_1 \cdot \mathbf{I}_1 + \mathbf{S}_2 \cdot \mathbf{A}_2 \cdot \mathbf{I}_2, \quad (10)$$

where  $\mathbf{g}_1$  and  $\mathbf{g}_2$  are the gyromagnetic tensors and  $\mathbf{A}_1$  and  $\mathbf{A}_2$  the hyperfine tensors for each site.  $\mathbf{H}$  is the applied magnetic field, and  $\mu_B$  is the Bohr magneton.

As a first approximation, the ESR data were used to calculate the  $\mathbf{g}$  and  $\mathbf{A}$  tensors by Schonland's method [17], and the obtained parameters were used as preliminary information for the subsequent calculation. The resonant field for each transition was obtained exactly, within the machine error, by diagonalizing numerically the  $16 \times 16$  matrix corresponding to each of the sites in Eq. (10), and obtaining the field self-consistently. These fields were the input to a least squares fitting program, treating the  $\mathbf{g}$ 's and  $\mathbf{A}$ 's values as adjusting parameters. All the experimental data of the three planes were fed in the program, and the solid lines in Figure 3 are the best fitting of the data using Eq. (10), and Table I gives the spin-Hamiltonian parameters obtained by this procedure.

In this compound the  $\text{Co}^{2+}$  ions are coordinated by six O in fairly regular octahedra [18]. Assuming that the position of the six oxygen nearest to the  $\text{Co}^{2+}$  are the same as those of

		$\cos(\theta_1)$	$\cos(\theta_2)$	$\cos(\theta_3)$
$g_1$	4.9091	-0.26072	-0.55762	0.78809
$g_2$	5.1389	0.96461	-0.11704	0.23630
$g_3$	2.6680	-0.03953	0.82180	0.56840
	$\times 10^{-4} \text{ cm}^{-1}$	$\cos(\theta_1)$	$\cos(\theta_2)$	$\cos(\theta_3)$
$A_1$	160.17	-0.20229	-0.58951	0.78202
$A_2$	178.76	0.97741	-0.07163	0.19884
$A_3$	44.37	-0.06120	0.80458	0.59068

TABLE I: Spin-Hamiltonian parameters for  $\text{Co}^{2+}$  in  $\text{NH}_4\text{NiPO}_4 \cdot 6\text{H}_2\text{O}$  at 4.2 K. The direction cosines are referred to the orthorhombic axes **a,b,c** of the crystal

Axes	a	b	c
j=x	0.7328	-0.3099	-0.6058
j=y	-0.00048	0.8900	-0.4559
j=z	0.6804	0.3344	0.6521

TABLE II: The cosines between the orthorhombic axes **a,b,c** of the crystal and the new axes j=x,y,z fixed to the octahedron, as discussed in the text.

the Nickel compound [18], and taking the average of their positions as the center of the octahedron, we choose two of the O and use them to determine an orthogonal system of axis. In the new system the  $x$  axis goes through the position of one of those two O, and the  $z$  axis is perpendicular to the plane determined by the two O and the center of the octahedron. The direction cosines of these axes with respect to the orthorhombic axis of the crystal are given in Table II. The average distance of the six O with respect to the origin of the new axes is  $\bar{R} = 2.0531\text{\AA}$ , and we can define a regular octahedron with the six vertices placed along the axes at a distance  $\pm\bar{R}$  from the origin.

To analyze further the experimental  $g$  tensor, one could try and find crystal field values that would reproduce the measured results, and a study of this type was presented by Abragam and Pryce for the Cobalt Tutton salts [19]. To simplify the study we present a model that describes all the crystal fields acting on the Co as originating in the crystal field of the six nearest O located at the vertices of a deformed octahedron, obtained by displacement of the vertices of the regular octahedron introduced at the beginning of this section. To organize the study, we employ Eq. (5) to express the crystal field as a function of the normal coordinates  $Q_j$  of the octahedron.

We shall use second order perturbation theory, using both  $V(\mathbf{r})$  and the Zeeman term  $H_Z = (g_e \mathbf{S} + \mathbf{L}) \cdot \mathbf{H}$  as perturbation. The change in the  $g$  tensor is then obtained from

$$\mathbf{S} \cdot \delta \mathbf{g} \cdot \mathbf{H} = \frac{2}{3} (g_e + \alpha) \frac{\mu_B}{\Delta} - C_E \left[ \sqrt{3} Q_2 (S_x H_x - S_y H_y) + Q_3 (3 S_z H_z - \mathbf{S} \cdot \mathbf{H}) \right] + C_T [Q_4 (S_z H_y + S_y H_z) + Q_5 (S_x H_z + S_z H_x) + Q_6 (S_x H_y + S_y H_x)], \quad (11)$$

where  $\mu_B$  is the Bohr magneton and  $\Delta$  is the splitting between the  $\Gamma_6$  doublet and the lowest  $\Gamma_8$  quadruplet in the octahedral

symmetry, given by [20]

$$\Delta = 1.5 (-1.5 a^2 + b^2) k_0 \lambda - \frac{33}{20} \left( \frac{\sqrt{15}}{2} a + b \right)^2 k_0^2 \frac{\lambda^2}{\Delta'} \quad (12)$$

The constants  $C_E$  and  $C_T$  can be obtained by calculating a single matrix element in each case:

$$C_E = -\frac{1}{2} \left\langle T_{1z} \left| \sum_j V_3(\mathbf{r}_j) \right| T_{1z} \right\rangle \quad (13)$$

and

$$C_T = \left\langle T_{1x} \left| \sum_j V_3(\mathbf{r}_j) \right| T_{1y} \right\rangle, \quad (14)$$

where the  $\{|T_{1x}\rangle, |T_{1y}\rangle, |T_{1z}\rangle\}$  are a basis of the ground  $^4T_1$  that transforms like the coordinates  $\{x, y, z\}$  under the octahedral group.

The expression in Eq. (11) corresponds to deformations from a cubic environment, and one should then compare this formula with the experimental  $g$  tensor in the axis of the regular octahedron defined in Table II, which is given in Table IV, but it is first necessary to determine  $C_E$  and  $C_T$ . One obtains with Eqs. (5-8)

$$C_E = \frac{e e_{eff}}{\bar{R}^2} (1.4846 - 1.7815 a^2 + 1.7815 a b - 0.4454 b^2) \frac{\langle r^2 \rangle}{\bar{R}^2} + (-0.1718 + 0.6873 a^2 - (0.6873 a b + 0.1718 b^2) \frac{\langle r^4 \rangle}{\bar{R}^4}) \quad (15)$$

and

$$C_T = \frac{e e_{eff}}{\bar{R}^2} \left\{ (0.0857 a^2 - 1.3714 a b + 1.2 b^2) \frac{\langle r^2 \rangle}{\bar{R}^2} + (-0.7143 a^2 - 0.2381 a b) \frac{\langle r^4 \rangle}{\bar{R}^4} \right\} \quad (16)$$

The averages  $\langle r^2 \rangle = 1.251$  and  $\langle r^4 \rangle = 3.655$  (atomic units) have been calculated with Hartree Fock functions [11], but we can obtain  $e_{eff} \langle r^4 \rangle$  from the cubic field parameter  $Dq$  employing the relation

$$Dq = -\frac{1}{6} \frac{e e_{eff} \langle r^4 \rangle}{\bar{R}^4} \quad (17)$$

valid for the point charge model. To find  $e_{eff} \langle r^2 \rangle$  we shall assume that  $\langle r^2 \rangle / \sqrt{\langle r^4 \rangle} = 0.6544$ , i.e. equal to the corresponding ratio obtained from the calculated values. Taking the  $B$  and  $Dq$  of the Ni compound and using for the remaining parameters those discussed in the text, one finds  $C_E = 6508 \text{ cm}^{-1}/\text{\AA}$  and  $C_T = -3414 \text{ cm}^{-1}/\text{\AA}$  while for the Co : MgO values one finds  $C_E = 6821 \text{ cm}^{-1}/\text{\AA}$  and

	$Q_2$	$Q_3$	$Q_4$	$Q_5$	$Q_6$
1	-0.03840	0.02497	0.01417	0.06542	-0.01275
2	0.01092	0.00305	0.16028	-0.22616	-0.14710
3	1.60	845.	2.04	1.77	1.99

TABLE III: The symmetrical normal coordinates of the complex formed by the Co and the six O with respect to the regular octahedron defined in the text. Row 1 gives the values calculated from the O positions determined crystallographically. Row 2 gives the values that would reproduce the experimental g tensor for the point charge model. Row 3 gives a number proportional to the ratio of the normal coordinates obtained from the g tensor divided into those obtained from the A tensor.

Axes	$g_{j,x}$	$g_{j,y}$	$g_{j,z}$
j=x	-0.1306	0.6354	0.9769
j=y	0.6354	0.1809	-0.6923
j=z	0.9769	-0.6923	-0.0503

TABLE IV: The components of the experimental g tensor, referred to the octahedron axes j=x,y,z, after subtraction of the isotropic tensor  $g=4.2387$ .

$C_T = -3932 \text{ cm}^{-1}/\text{\AA}$ . The difference is not critical, and we shall use the Ni values in the remaining of the discussion.

It is now possible to compare Eq. (11) with Table IV, and one immediately obtains values of the normal coordinates that would reproduce the experimental g tensor when substituted in that equation. These values are given in the second line of Table III, and it is clear that they are rather different from the values calculated from the crystallographic position of the O in the Ni compound. There are two alternative explanations for this result: either the O around the Co impurity are in different positions than in the Ni compound, or the model is not adequate. In the absence of experimental evidence to check the first alternative, we shall discuss possible modification to the model employed above. Instead of the point charge model we could use a model with dipoles, all “directed away from the central ion”[4]. This model gives the same potential of Eqs. (5-7) but with different expression for the constants  $A, B, C, E$ . Within each irreducible representations  $E$  and  $T_2$ , the normal coordinates necessary to reproduce the g tensor would then be proportional to those obtained with the point charge model, as only the values of  $C_E$  and  $C_T$  would change in this model, so that both the charge and dipole models would give essentially the same results. A more complicated model, either involving the change in the direction of the dipoles, or even considering the extended charges of the ligands, would increase very much the difficulty of the calculation. We should then remain with the point charge model, but only as a means to obtain a fairly simple crystal field that would be sufficient to explain the experimental g tensor. This crystal field is the  $V(\mathbf{r})$  of Eq. (5) given in the axes of the regular octahedron defined in Table II with the  $Q_j$  given in the second row of Table III. The agreement is perfect because there are as many free normal coordinates as  $\delta g$  components, but the point charge model employed should not be taken too seriously.

Although we have not analyzed the hyperfine tensor in detail, we can extract some information from its experimental

Axes	$A_{j,x}$	$A_{j,y}$	$A_{j,z}$
j=x	-970.	3200.	5510.
j=y	3200.	970.	-3390.
j=z	5510.	-3390.	0.

TABLE V: The components of the experimental A tensor (given in  $\text{cm}^{-1}$ ), referred to the octahedron axes j=x,y,z, after subtraction of the isotropic tensor  $A = 12780 \text{ cm}^{-1}$ .

value. As seen from Table I, the principal axes of the two tensors g and A do not exactly coincide, but are fairly close together. As with the g tensor, we have expressed the  $\delta A$  tensor in the axes of the regular octahedron discussed above, and the corresponding values are given in Table V. One can show [21] that the  $\delta A$  is described by an expression similar to that of the  $\delta g$  (cf. Eq. (11)) with the component of  $\mathbf{I}$  taking the place of the components of  $\mathbf{H}$ , but we have not explicitly calculated the coefficients equivalent to the  $C_E$  and  $C_T$ . Nevertheless, by the same method employed with the g tensor one can obtain quantities  $Q'_j$  proportional the  $Q_j$ , and then calculate the ratio of the  $Q'_j$  given in the second row of Table III to the corresponding  $Q'_j$  obtained from the A tensor. These ratios are given in the third row of Table III, and those corresponding to  $Q_j$  of the same irreducible representation should be equal if the theory were strictly true. The enormous value of the ratio corresponding to  $Q_3$  is not significant, because the value derived from the A tensor is zero within the experimental error, and one can therefore not draw any conclusions from the pair  $\{Q_2, Q_3\}$ . On the other hand, the three ratios corresponding to  $\{Q_4, Q_5, Q_6\}$  are fairly close to the same value, and they show that the crystal fields that result from the present treatment are fairly consistent with the available experimental results.

In the present calculation we have neglected the effect of the  $^4T_2$  triplet, that contributes to  $\delta g$  in third order perturbation (our calculation would be of the second order). This effect was calculated by Tucker[11] who obtained contributions that are about 6% of the second order contribution for the  $T_2$  deformation and about 13% for the  $E$  deformation, and would therefore not alter substantially our conclusions.

A similar treatment of the  $\text{Co}^{2+}$  in sites with deformed octahedral symmetry of  $\text{Co}_2(\text{OH})\text{PO}_4$  or  $\text{Co}_2(\text{OH})\text{AsO}_4$  has been considered in [3], but it is less interesting because only the powder samples of these compounds have been measured. The treatment of this problem shall not be further discussed in the present work.

We conclude that employing the normal modes of the seven ion complex to adjust the values of the g-factor tensor, it is possible to estimate the crystal fields of the whole crystal acting on the  $\text{Co}^{2+}$  impurity ion.

#### IV. THE $\text{Co}^{2+}$ IN A DEFORMED TRIGONAL BIPYRAMID

In this section we shall study two members of the adamite family, which takes its name from the natural compound [22, 23]  $\text{Zn}_2(\text{OH})\text{AsO}_4$ . The cations can occupy two sites with rather different environments in this compound, one being octahedral and the other penta-coordinated, so that rather dif-

ferent magnetic properties could be expected when magnetic cations are employed. The recently synthesized compounds  $\text{Zn}_2(\text{OH})\text{PO}_4$  [24],  $\text{Co}_2(\text{OH})\text{PO}_4$  [24],  $\text{Mg}_2(\text{OH})\text{AsO}_4$  [25, 26], as well as the natural  $\text{Co}_2(\text{OH})\text{AsO}_4$  [27], present these two type of sites. We have then found interesting to study the properties of the  $\text{Co}^{2+}$  ions as impurities in the two non-magnetic compounds, as a first step in the understanding of the properties of the concentrated compounds.

To analyze the ESR measurements it is necessary to have information about the splitting of the energy levels with both the crystal field and the electronic Coulomb repulsion, and we obtained this information from optical diffuse reflectance measurements [28].

The experimental ESR powder spectra of  $\text{Co}^{2+}$  impurities in both  $\text{Zn}_2(\text{OH})\text{PO}_4$  and  $\text{Mg}_2(\text{OH})\text{AsO}_4$  present two different sets of lines, one very intense, and the other just observable. The average of the  $g$  factors of the intense spectra is 4.15 in the two compounds, a value close to the 4.33 expected for  $\text{Co}^{2+}$  in moderately distorted octahedral symmetry [29], and it seems reasonable to assign these spectra to that environment and apply the same approach employed in the previous section in the study of the ESR of  $\text{Co}^{2+}$  in  $\text{NH}_4\text{NiPO}_4 \cdot 6\text{H}_2\text{O}$  (see also [2]). The remaining lines are very weak and we assign them to the penta-coordinated symmetry (the possible reason for their small intensity has been discussed in [3]).

Here we shall only briefly consider the deformed octahedral symmetry, and give more details of the theory describing the ESR of  $\text{Co}^{2+}$  in the penta-coordinated environment, that was partially discussed in [3]. This last complex is a distorted trigonal bipyramid, and we first calculated the crystal fields of the perfect trigonal bipyramid following the existing literature [30, 31]. To analyze the distorted complex we derived the normal modes of the trigonal bipyramid with respect to the reference complex, and then obtained the Jahn-Teller contributions [7, 8] to the crystal field acting on the  $\text{Co}^{2+}$ , that is generated by these modes.

In this calculation we have introduced a procedure that uniquely defines the orientation and size of the two reference complexes, so that the normal modes that describe their deformation are free from irrelevant rotations and expansions.

These results were then employed to analyse the theoretical ESR spectra. We found that for the system parameters obtained from the optical spectra we should expect that the ground doublet be  $M_J = \pm 1/2$ , corresponding to an allowed spectrum. The rather small intensity, of this type of spectra seems to indicate a preference of  $\text{Co}^{2+}$  for the octahedral sites in the crystal structure, a conjecture that was advanced in a preliminary report [32] on the ESR of impurities of this ion in  $\text{Mg}_2(\text{OH})\text{AsO}_4$ , and was confirmed in [3]. Employing a molecular calculation we have verified in the last reference that the formation energies of the two type of complexes, with both Co and Zn as the central ions, are compatible with this hypothesis.

${}^4T_{1g} \rightarrow {}^4T_{2g}$	${}^4A_{2g}$	${}^4T_{1g}(P)$	$B$	$D_q$
PO <sub>4</sub>				
a)	8450	15450	18350	
b)	7819	16013	18324	767.6 819.4
AsO <sub>4</sub>				
a)	7700	15500	18020	
b)	7616	15585	18011	758.9 796.9

TABLE VI: a) The transitions between the ground  ${}^4T_{1g}$  level and the levels shown at the top of each column, in  $\text{cm}^{-1}$  and assigned from the experimental spectra of the octahedral complexes of  $\text{Co}_2(\text{OH})\text{PO}_4$  and  $\text{Co}_2(\text{OH})\text{AsO}_4$ ; the level  ${}^4T_{1g}(P)$  corresponds to the highest of the same symmetry. b) The best fit, obtained with the  $B$  and  $D_q$  shown in the last two columns.

${}^4A'_2 \rightarrow {}^4A'_1, {}^4A''_2$	${}^4E''$	${}^4E'$	${}^4A'_2(P)$	${}^4E''(P)$
PO <sub>4</sub>				
a)	6400	7000	11100	15800 19600
b)	3233	4835	12868	17386 17947
c)	1511	3603	11106	15801 19604
AsO <sub>4</sub>				
a)	5000	6250	10870	16000 19800
b)	2707	4440	12210	17188 18595
c)	1437	3535	10876	15999 19805

TABLE VII: a) The transitions between the ground level  ${}^4A'_1$  and the levels shown at the top of each column, given in  $\text{cm}^{-1}$  and assigned from the experimental spectra of the penta-coordinated complexes of  $\text{Co}_2(\text{OH})\text{PO}_4$  and  $\text{Co}_2(\text{OH})\text{AsO}_4$ . b) The best possible fit to the five transitions. c) The best fit obtained by adjusting only the three transitions of higher energy. The corresponding values of  $B$ ,  $D_s$ ,  $D_t$  are given in rows b) and c) of table XV.

### A. Optical studies.

The necessary optical data was obtained from diffuse reflectance experiments in the  $5000 - 50000 \text{ cm}^{-1}$  wavenumber region [3, 28, 33]. The whole of the optical data used in this work was recorded at room temperatures, and all the relevant data that was necessary in the present work is in the tables VI and VII. The system parameters of the octahedral complexes are slightly different from those already published [28, 33], because they were obtained from the optical spectra after including a spin orbit correction in the ground orbital level [34].

### B. Electron Spin Resonance (ESR).

The measurement of the ESR of  $\text{Co}^{2+}$  impurities in both  $\text{Zn}_2(\text{OH})\text{PO}_4$  and  $\text{Mg}_2(\text{OH})\text{AsO}_4$  has been discussed in [3], and some of the measured ESR spectra for the two samples are reproduced in Figs. 4 and 5. Only powder spectra could be measured for the two systems because it was not possible to obtain single crystals, and small concentrations of Co (1% in the arsenate and 0.1% in the phosphate) substitute the metals in the two lattices. The curves denoted with (a) in Figs. 4 and 5 show the measured spectra for the two samples, recorded at 4.2 K, and they both clearly show three sets of lines with a well

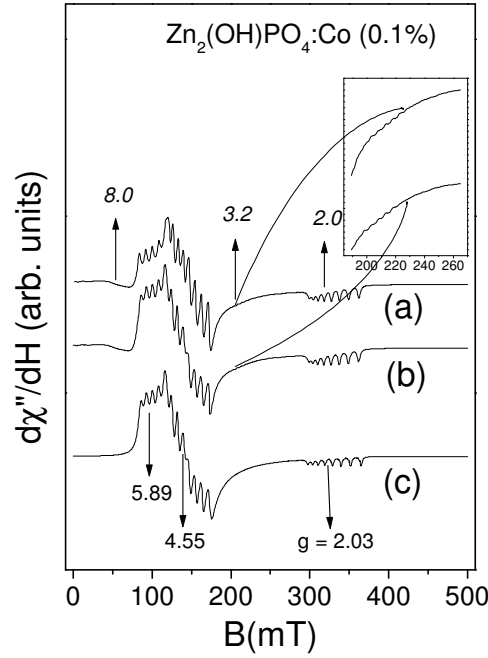


FIG. 4: ESR spectra of  $\text{Co}^{2+}$  in  $\text{Zn}_2(\text{OH})\text{PO}_4$ . a) Experimental spectrum. b) Sum of the simulated spectrum for both the hexa-coordinated and penta-coordinated complexes. c) Simulated spectrum for the hexa-coordinated complex. The  $g$ -values of both the octahedral and of the penta-coordinated complexes are given in table VIII. The arrows in c) show the  $g$ -values and their positions for the octahedral complex, while those in a) correspond to the penta-coordinated complex. The insert gives the detail of the experimental hyperfine structure and of the simulated one (around  $g_2$ ), attributed to the  $\text{Co}^{2+}$  in the triangular bipyramid.

defined hyperfine structure that identifies the  $\text{Co}^{2+}$  ion. There are also some extra lines, rather weak in the phosphate but more intense in the arsenate, that preclude an automatic fitting of the spectra, and the powder spectra of the hexa-coordinated  $\text{Co}^{2+}$  were simulated with a more flexible program. The best results, plotted in the curves (c) of Figs. 4 and 5, correspond to the  $g$ -values shown in rows a) of table VIII. Their values and positions are also shown by arrows below the simulated curves (c). The extra lines near 200 mT in the phosphate show an hyperfine structure typical of the  $\text{Co}^{2+}$ , and are given in more detail in the inset of Fig. 4. The remaining lines in the two compounds are rather broad and show a collapsed hyperfine structure. The curves (b) in the Figs. 4 and 5 show the sum of the simulated spectra of the hexa-coordinated  $\text{Co}^{2+}$  in (c), plus a simulation of the penta-coordinated  $\text{Co}^{2+}$  that employs the  $g$ -values given in rows b) of table VIII and is adequately renormalized to account for the smaller relative concentration of the last compound. These  $g$  values have rather large errors, and their positions are shown by arrows above the measured spectra (a) of Figs. 4 and 5. In the inset of Fig. 4 it is also shown the detail of the hyperfine structure near 200 mT both in the experimental and in the simulated spectrum.

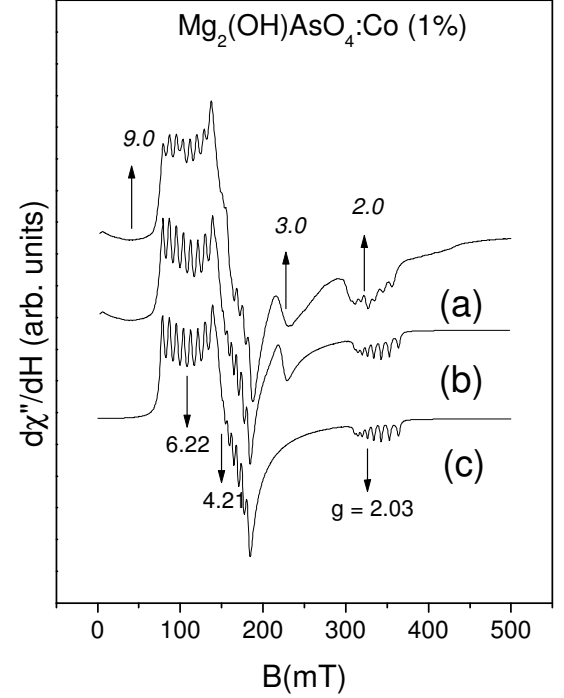


FIG. 5: ESR spectra of  $\text{Co}^{2+}$  in  $\text{Mg}_2(\text{OH})\text{AsO}_4$ . Curves a), b), and c), and the meaning of the arrows and values in curves a) and c) are the same as in figure 4.

	$g_1$	$g_2$	$g_3$	$A_1$	$A_2$	$A_3$
<b>PO<sub>4</sub></b>						
a	$5.89 \pm 0.02$	$4.55 \pm 0.05$	$2.02 \pm 0.02$	$240 \pm 5$	$155 \pm 8$	$85 \pm 3$
b	$8. \pm 0.5$	$3.2 \pm 0.3$	$2.0 \pm 0.2$			
<b>AsO<sub>4</sub></b>						
a	$6.22 \pm 0.02$	$4.21 \pm 0.05$	$2.05 \pm 0.02$	$140 \pm 5$	$120 \pm 7$	$55 \pm 5$
b	$9. \pm 1.5$	$3. \pm 0.5$	$2.0 \pm 0.2$			

TABLE VIII: Values of the principal  $g$  and  $A$  parameters, obtained from the spectra in Figs. 4 and 5. The values of the  $A$  parameters are in  $10^{-4} \text{ cm}^{-1}$  units. a) Octahedral complex: the  $g$  and  $A$  values were obtained from a program simulating powder spectra, as described in the text. b) The parameters for the penta-coordinated  $\text{Co}^{2+}$ , also estimated by simulation.

### C. Hexa-coordinated Co

We shall briefly discuss the hexa-coordinated  $\text{Co}^{2+}$  ions in  $\text{Zn}_2(\text{OH})\text{PO}_4$  and  $\text{Mg}_2(\text{OH})\text{AsO}_4$  following the same treatment employed in Section III. The  $\text{Co}^{2+}$  is surrounded by six oxygens in a fairly regular octahedron with positions given in table IX, and only powder spectra were available. The three principal values  $g_i$  of the  $\mathbf{g}$  tensor could be measured, but without all the details obtained for the  $\text{NH}_4\text{NiPO}_4 \cdot 6\text{H}_2\text{O}$  compound (see table VIII).

As before we shall consider the effect that the crystal field generated by the normal modes of the octahedron has on the



n	a (Å)	b (Å)	c (Å)	a (Å)	b (Å)	c (Å)
PO <sub>4</sub>			AsO <sub>4</sub>			
1	4.7150	-1.2420	0.0000	0.9197	-1.0794	0.0000
2	4.9627	-1.0327	2.9700	0.6438	-1.2633	3.0255
3	2.1592	-1.2713	1.7274	-1.9091	-1.1662	1.3476
4	3.0793	1.0327	2.9700	-0.6438	1.2633	3.0255
5	3.3270	1.2420	0.0000	-0.9197	1.0794	0.0000
6	5.8827	1.2713	1.7274	1.9091	1.1662	1.3476
7	4.0210	0.0000	1.5135	0.0000	0.0000	1.4910

TABLE IX: The columns **a,b,c** give the position of the six oxygens (n=1,...,6) and Cobalt (n=7) in the hexa-coordinated complexes of Co<sub>2</sub>(OH)PO<sub>4</sub> and Co<sub>2</sub>(OH)AsO<sub>4</sub> with respect to the three unit cell axes. The X,Y,Z axes roughly correspond to n=1,2,3 respectively, taking n=7 as the origin.

	Q <sub>2</sub> /R	Q <sub>3</sub> /R	Q <sub>4</sub> /R	Q <sub>5</sub> /R	Q <sub>6</sub> /R
PO <sub>4</sub>					
a)	0	-0.04407	0.03478	0.03478	0.11425
b)	0	-0.11683	-0.01717	-0.01717	-0.05641
AsO <sub>4</sub>					
a)	0	-0.0441	0.04032	0.04032	0.09989
b)	0	-0.09328	-0.02818	-0.02818	-0.06982

TABLE X: Normal modes of the octahedral Co divided by the Co-O distance  $R$  in Co:Zn<sub>2</sub>(OH)PO<sub>4</sub> and Co:Mg<sub>2</sub>(OH)AsO<sub>4</sub>. a) Values that adjust the experimental values of the  $g$  tensor. b) Values obtained from the crystallographic positions corresponding to the pure compounds.

gyromagnetic tensor  $\mathbf{g}$ . This method systematizes the procedure, and in table X we give the normal modes that reproduce the experimental values of the three  $g_i$ . We shall then choose a reference perfect octahedron centered in the Co<sup>2+</sup>, calculate the normal modes corresponding to the crystallographic positions of the O, and compare them in table X with those obtained from the experimental spectra.

The average values of  $g$  are 4.1537 for Co:Zn<sub>2</sub>(OH)PO<sub>4</sub> and 4.153 for Co:Mg<sub>2</sub>(OH)AsO<sub>4</sub>, and to analyse these results it is sufficient to consider the Co<sup>2+</sup> in pure octahedral symmetry, because the crystal fields of lower symmetry do not change this value in our approximation. The calculation follows the same lines given in reference[2] and shall not be repeated here.

The values of the constants  $a$  and  $b$  that give the mixture of the ground <sup>4</sup> $F$  with the lowest <sup>4</sup> $P$  can be obtained as before from the Racah parameter  $B$  and the crystal field parameter  $D_q$ , that were estimated [34] from the spectroscopic

	X	Y	Z	X	Y	Z
PO <sub>4</sub>			AsO <sub>4</sub>			
a	0.4054	-0.5794	-0.7071	0.3800	-0.5963	-0.7071
b	0.4054	-0.5794	0.7071	0.3800	-0.5963	0.7071
c	-0.8194	-0.5733	0.0000	-0.8434	-0.5373	0.0000

TABLE XI: Direction cosines of the three axis **X,Y,Z** of the reference perfect octahedron of Co<sub>2</sub>(OH)PO<sub>4</sub> and Co<sub>2</sub>(OH)AsO<sub>4</sub> with respect to the three crystallographic axis **a, b, c**

data and are given in table VI. With these values one obtains  $a = -0.9820$  and  $b = 0.1886$  for the phosphate, and the proportionality constant of the angular momentum is then

$$\alpha = -1.5 a^2 + b^2 = -1.4110. \quad (18)$$

As discussed in Section III we use Eq. (11) to relate the change  $\delta \mathbf{g}$  in the  $g$  tensor with the normal modes  $Q_j$  of the complex of Co<sup>2+</sup> with the six neighboring O, employing  $\Delta = 283 \text{ cm}^{-1}$  as the splitting between the  $\Gamma_6$  doublet and the lowest  $\Gamma_8$  quadruplet in the octahedral symmetry in the P compound.

The values of  $C_E$  and  $C_T$  are obtained by the same procedure employed in Section III. For the Co-O distance  $R$  we used  $R = 2.11176 \text{ Å}$ , corresponding to the reference octahedron defined below, and we found the values  $C_E = 6436 \text{ cm}^{-1}/\text{Å}$  and  $C_T = -3666 \text{ cm}^{-1}/\text{Å}$ . We can now calculate the crystal fields that would describe the experimental values of  $\mathbf{g}$  or, what is equivalent, the corresponding normal modes within the approximations just discussed. As there are more normal modes than data, we fix the relations  $Q_4 = Q_3 = 0.3044 Q_6$ , which correspond to the normal modes calculated below from the crystallographic positions, and we obtain a perfect fit to the experimental values employing the normal modes given table X.

From table VI we obtain the coefficients  $a = -0.9824$ ,  $b = 0.1867$ , and  $\alpha = -1.4128$  for Co<sub>2</sub>(OH)AsO<sub>4</sub>. The ESR data was then adjusted with the normal modes coordinates given in table X, where we used  $R = 2.1224 \text{ Å}$ ,  $Q_4 = Q_3 = 0.4037 Q_6$ ,  $C_E = 6287 \text{ cm}^{-1}/\text{Å}$ ,  $C_T = -3558 \text{ cm}^{-1}/\text{Å}$  and  $\Delta = 282 \text{ cm}^{-1}$ , for this compound.

To calculate the crystallographic normal modes of the octahedron it is necessary to chose a reference perfect octahedron centered in the Co<sup>2+</sup>. To this purpose we consider the three normal modes of pure rotation, [4]  $Q_{19}$ ,  $Q_{20}$ , and  $Q_{21}$ , and we chose the axes of the reference octahedron so that these three normal coordinates are zero, because they should not have any effect on the properties of the complex. The value  $R = 2.11176 \text{ Å}$  of the Co-O distance in the reference octahedron was chosen so that  $Q_1 = 0$ , and by this whole procedure we obtain a unique reference octahedron and minimize the effect of irrelevant rotations and expansions on the values of the normal modes. The direction cosines of the three Co-O directions in the reference octahedron are given in table XI, and the normal modes derived from the crystallographic ionic positions given in table IX are shown in the third line of table X. The normal modes calculated from the crystallographic position of the O in the octahedral complex are different than those obtained from the experimental  $\mathbf{g}$  tensor, given in the first line of the same table. This result indicates that although the nearest O to the Co are the main source of the cubic field [4], the remaining non-cubic perturbations have strong contributions due to the rest of the crystal. We conclude that the experimental  $\mathbf{g}$  tensor could be explained by the crystal field  $V(\mathbf{r})$  of Eq. (11) given in the axes of the reference octahedron defined in table XI with the  $Q_j$  given in the row a) of table X. The agreement is perfect because there are more free normal coordinates than available  $\delta \mathbf{g}$  components, but the theory presented can only be considered a first approximation. In

particular, although the crystal field theory of point charges gives the right symmetry properties, it is only a very rough description of the physics of the problem, but the crystal field  $V(\mathbf{r})$  obtained give a much better description of the system than the model employed.

Although we have not analyzed the hyperfine tensor in detail, we have verified that its components are compatible with the normal modes necessary to describe the  $\delta\mathbf{g}$  tensor.

In the present calculation we have neglected the effect of the  $^4T_2$  triplet, that contributes to  $\delta\mathbf{g}$  in third order perturbation (our calculation is of the second order). This effect was calculated by Tucker[11] who obtained contributions that are about 6% of the second order contribution for the  $T_2$  deformation and about 13% for the  $E$  deformation, and would therefore not alter substantially our conclusions.

#### D. Penta-coordinated Co

##### 1. The crystal field of the trigonal bipyramid.

The structure of the penta-coordinated complex of  $\text{Co}^{2+}$  is very close to a trigonal bipyramid, and the positions of the Co and of the five O are given with respect to the crystal axes in table XII. Following a method similar to that employed in the octahedral case we chose an orthogonal system of axes X,Y,Z, such that the normal modes obtained from the crystallographic positions would not have contributions of irrelevant rotations and expansions. The direction cosines of the axes of this system with respect to the crystal axes **a**, **b** and **c** are given in table XIII, and the coordinates of the six atoms in the reference perfect trigonal bipyramid are given in table XIV. There are two different Co-O distances in the reference complex:  $R_a$  corresponds to the three ligands in the XY plane (equatorial O) and  $R_c$  to the two along the Z axis (axial O); their values for the phosphate and arsenate are given in the caption of table XIV. Two crystal field parameters  $D_s$  and  $D_t$  are necessary in the trigonal bipyramid, and are given in the point charge model [30, 35] by:

$$\begin{aligned} D_s &= \frac{e}{14} \left[ \frac{4q_c}{R_c^3} - \frac{3q_a}{R_a^3} \right] \langle r^2 \rangle, \\ D_t &= \frac{e}{168} \left[ \frac{16q_c}{R_c^5} + \frac{9q_a}{R_a^5} \right] \langle r^4 \rangle, \end{aligned} \quad (19)$$

where we shall use  $q_a = q_c = -2e$ . The crystal field potential  $V_{cf}$  can be expressed by the usual formula

$$V_{cf}(\mathbf{r}) = \sum_{kq} \sqrt{\frac{4\pi}{2k+1}} \sum_{\ell} q_{\ell} \frac{r_{\ell}^k}{r_{\ell}^{k+1}} Y_{kq}^*(\theta_{\ell}, \varphi_{\ell}) C_q^{(k)}(\theta, \varphi), \quad (20)$$

where  $Y_{kq}(\theta_{\ell}, \varphi_{\ell})$  are the spherical harmonics at the position of the  $\ell$ -th ligand and the  $C_q^{(k)}(\theta, \varphi) = \sqrt{4\pi/(2k+1)} Y_{kq}(\theta, \varphi)$  are usually called the Racah's rationalized spherical harmonics. In our actual calculation we have employed the real combinations  $C_{lm}(\theta, \varphi)$  and  $S_{lm}(\theta, \varphi)$  that are proportional

n	a (Å)	b (Å)	c (Å)	a (Å)	b (Å)	c (Å)
	PO <sub>4</sub>			AsO <sub>4</sub>		
1	4.9008	3.2438	2.9700	4.9744	0.9132	3.0180
2	1.8617	2.9132	1.2426	1.9003	1.1604	1.3442
3	1.8617	2.9132	4.6974	1.9003	1.1604	4.6676
4	3.1412	5.1252	2.9700	3.2085	3.2015	3.0180
5	3.0793	1.0327	2.9700	3.2736	-0.9132	3.0180
6	2.9102	3.0621	2.9700	3.0056	1.1561	3.0180

TABLE XII: The columns **a,b,c** give the position of the five oxygens (n=1,...,5) and Cobalt (n=6) in the penta-coordinated complexes of  $\text{Co}_2(\text{OH})\text{PO}_4$  and  $\text{Co}_2(\text{OH})\text{AsO}_4$  with respect to the three unit cell axes.

	X	Y	Z	X	Y	Z
	PO <sub>4</sub>			AsO <sub>4</sub>		
<b>a</b>	0.	0.	1.	-0.00203	0.	0.999998
<b>b</b>	0.99931	0.03720	0.	0.999698	-0.02449	0.00203
<b>c</b>	-0.03720	0.99931	0.	0.02449	0.9997	0.00005

TABLE XIII: Direction cosines of the three axis **X,Y,Z** employed to define the reference perfect trigonal bipyramid of  $\text{Co}_2(\text{OH})\text{PO}_4$  and  $\text{Co}_2(\text{OH})\text{AsO}_4$  with respect to the three crystallographic axis **a, b, c**

to  $\cos(m, \varphi)$  and  $\sin(m, \varphi)$  respectively [36]. In the absence of the spin-orbit interactions one employs the irreducible representations  $\Gamma$  of the trigonal bipyramid to classify the eigenstates  $|\alpha, S, L, \Gamma, \gamma, a\rangle$  of the Hamiltonian, which are simply related to the states  $|\alpha, S, L, M_L\rangle$  (the index  $\alpha$  identifies the particular states with the same  $S, L$ ). In table I of reference 30 we find that the irreducible representations  $A'_2, A''_1, A''_2, E'$  and  $E''$  are contained in the two terms  $^4F$  and  $^4P$ , and that the  $|\alpha, S, L, M_L\rangle$  states that generate the corresponding subspaces are  $\{|3, 3/2, 3, 0\rangle, |3, 3/2, 1, 0\rangle\} \rightarrow A'_2$ ,  $\{|3, 3/2, 3, \pm 3\rangle\} \rightarrow (A''_1, A''_2)$ ,  $\{|3, 3/2, 3, \pm 2\rangle\} \rightarrow E'$  and  $\{|3, 3/2, 3, \pm 1\rangle, |3, 3/2, 1, \pm 1\rangle\} \rightarrow E''$ . The Hamiltonian without spin orbit interaction is diagonal in the partners  $\gamma$  of each irreducible representation  $\Gamma$  and in the spin component  $M_S$ , so it is not necessary to write them explicitly here. The only  $C_q^{(k)}(\theta, \varphi)$  that contribute to Eq.(20) in the perfect trigonal bipyramid have  $k = 0, 2, 4$  and  $q = 0$ . To calculate the matrix elements of the Hamiltonian that contains  $V_{CF} = \sum_{i=1,7} V_{cf}(\mathbf{r}_i)$ , we have used the standard tensorial operator techniques [37] as well as the unitary operators obtained from Nielsen and Koster's tables [37, 38], and we have verified that our matrix coincides with that given in table II or reference 30.

Our main objective here is to find the gyromagnetic factors that one would expect to measure in the penta-coordinated  $\text{Co}^{2+}$ , and we shall employ the spectroscopic data measured by diffuse reflectance to estimate the parameters  $B, D_s$  and  $D_t$  for both  $\text{Co:Zn}_2(\text{OH})\text{PO}_4$  and  $\text{Co:Mg}_2(\text{OH})\text{AsO}_4$ . In the two rows labelled a) of table VII we give the corresponding assignments of the transitions from the ground  $^4A'_2$  to the levels with symmetry  $^4A''_1, ^4A''_2, ^4E'', ^4E', ^4A'_2(P)$  and  $^4E''(P)$ , where we use  $(P)$  to indicate the higher levels of the same symmetry.

From the eigenvalues of the Hamiltonian in the absence of the spin-orbit interaction, we find by trial and error the values

n	X	Y	Z
1	0	$R_a$	0
2	$-\frac{\sqrt{3}}{2}R_a$	$-\frac{1}{2}R_a$	0
3	$\frac{\sqrt{3}}{2}R_a$	$\frac{1}{2}R_a$	0
4	0	0	$R_c$
5	0	0	$-R_c$
6	0	0	0

TABLE XIV: The columns X,Y,Z give the position of the five oxygens (n=1,...,5) and Cobalt (n=6) in the reference perfect penta-coordinated complexes of  $\text{Co}_2(\text{OH})\text{PO}_4$  [ $R_a = 2.01622 \text{ \AA}$  and  $R_c = 2.04365 \text{ \AA}$ ], and  $\text{Co}_2(\text{OH})\text{AsO}_4$  [ $R_a = 1.98578 \text{ \AA}$  and  $R_c = 2.05596 \text{ \AA}$ ] with respect to the axes defined in table XIII

	B	$D_s$	$D_t$	B	$D_s$	$D_t$
	PO <sub>4</sub>			AsO <sub>4</sub>		
b	728.	165.	947.	785.	313	919.
c	852.	745.	885.	875.	749.	869.

TABLE XV: The values of  $B$ ,  $D_s$ ,  $D_t$  in  $\text{cm}^{-1}$  that fit the optical transitions, given in table VII, of the two penta-coordinated complexes. The best fit to the five transitions is given in row b), and the best fit to the three highest transitions in row c). The spin orbit parameter  $\zeta = 580 \text{ cm}^{-1}$  was used in all these fittings

of  $B$ ,  $D_s$  and  $D_t$  that minimize the mean square deviation  $\chi$  for the two systems, and we give them in row b) of table XV. The transitions calculated with these two sets of values are given in the two rows of table VII that are labelled b). The fitting is rather poor, and in particular the transitions to the levels  $^4A_1''$ ,  $^4A_2'$  and  $^4E''$  fall below the range of the measuring equipment. As an alternative we have fitted only the three highest transitions, obtaining the values given in row c) of table XV, and the corresponding values calculated with these two sets of parameters are given in the two rows of table VII that are labelled c). In the following section we shall consider these two sets of values to estimate the gyromagnetic factors for each of the two compounds.

### 2. The spin-orbit interaction in the trigonal bipyramid.

It is now essential to include the spin orbit interaction into the calculation. The basis of the irreducible representations  $\Gamma_7$ ,  $\Gamma_8$  and  $\Gamma_9$ , of the double group  $D_{3h}^*$  have a simple expression in our system (cf. reference [31]): they are given by  $|d^7 \alpha SLJM_J\rangle$ , and in particular we have  $\Gamma_7(a) \equiv \{|d^7 \alpha SLJ \pm 1/2\rangle\}$ ,  $\Gamma_7(b) \equiv \{|d^7 \alpha SLJ \pm 11/2\rangle\}$ ,  $\Gamma_8(a) \equiv \{|d^7 \alpha SLJ \pm 5/2\rangle\}$ ,  $\Gamma_8(b) \equiv \{|d^7 \alpha SLJ \pm 7/2\rangle\}$ ,  $\Gamma_9(a) \equiv \{|d^7 \alpha SLJ \pm 3/2\rangle\}$  and  $\Gamma_9(b) \equiv \{|d^7 \alpha SLJ \pm 9/2\rangle\}$ . These states are easily obtained from the  $|d^7, \alpha, S, M_S, L, M_L\rangle$  calculated above by employing the 3-j or the Clebsch Gordan coefficients. In the absence of magnetic fields the two states of each Kramer's doublet have the same energy, and to calculate the energies of the system it is enough to consider only the states with positive  $M_J$ . As only the mixture of the  $^4F$  and  $^4P$  states is important in our problem we shall con-

sider only that subspace, and the corresponding matrix of the total Hamiltonian splits into five boxes of the following dimensions:  $(M_J = 1/2) \rightarrow \Gamma_7(a) \rightarrow (7 \times 7)$ ,  $(M_J = 3/2) \rightarrow \Gamma_9(a) \rightarrow (6 \times 6)$ ,  $(M_J = 5/2) \rightarrow \Gamma_8(a) \rightarrow (4 \times 4)$ ,  $(M_J = 7/2) \rightarrow \Gamma_8(b) \rightarrow (2 \times 2)$ ,  $(M_J = 9/2) \rightarrow \Gamma_9(b) \rightarrow (1 \times 1)$ , and there are no matrix elements of  $M_J = 11/2$ , i.e.  $\Gamma_7(b)$ , within the subspace  $\{^4F, ^4P\}$  of  $d^7$  that corresponds to  $S = 3/2$ . The matrices we have obtained coincide with those given in table II of reference 31, and their eigenvalues have been calculated for the different sets of  $B$ ,  $D_s$  and  $D_t$  values that were obtained above, employing the one-electron spin-orbit parameter  $\zeta = 580 \text{ cm}^{-1}$ . For all the set of parameters in table XV the lowest doublet is a  $\Gamma_7(a)$  ( $M_J = \pm 1/2$ ), separated by at least  $75 \text{ cm}^{-1}$  from the following  $\Gamma_9(a)$  ( $M_J = 3/2$ ) doublet, and by more than  $2377 \text{ cm}^{-1}$  from the remaining doublets. This situation is not altered by making fairly large changes in the three basic parameters  $B$ ,  $D_s$  and  $D_t$ , and shows that even for moderate increases in the temperature only the lowest doublet ( $M_J = \pm 1/2$ ) would be occupied. This doublet has allowed ESR transitions, and should be observed within the approximation employed. If the position of the two lowest doublets were exchanged, the ESR transitions of the lowest doublet would be forbidden and the spectra should not be then observed.

The fact that the two lowest doublets have  $M_J = \pm 1/2$  and  $M_J = \pm 3/2$  and are separated by a large energy from the remaining doublets is easily understood when we notice that the lowest level in the absence of spin-orbit interaction is  $^4A_2'$ . The orbital part  $A_2'$  is a singlet with no orbital angular momentum, and the total  $\mathbf{J}$  would then correspond to the  $S = 3/2$ . These four states would be rather far apart from the remaining ones, and would split in the way calculated above through the higher order spin orbit mixing with those excited states.

The present calculation was for a perfect trigonal bipyramid with  $D_{3h}$  symmetry, and one wonders whether the deformations with respect to this structure could alter the relative position of the two lowest doublets, thus changing from an allowed to a forbidden ESR transition. We shall then study the effect of these deformations, both on the relative position of the two lowest doublets and on the value of the gyromagnetic tensor. In this study we shall follow a treatment similar to that employed in the octahedral case, by considering the effect of the normal modes of the trigonal bipyramid on the Hamiltonian of the penta-coordinated  $\text{Co}^{2+}$ .

### 3. The normal modes of the trigonal bipyramid

As in the octahedral case we are interested in a contribution to the Hamiltonian of the same type of Eq. (5), but here the normal modes  $Q_j$  and  $V_j(\mathbf{r})$  transform like the same partners of irreducible representations of the trigonal bipyramid. As the undistorted complex does not have a center of symmetry, both the even and odd modes against reflection in the equatorial plane may have non-zero matrix elements inside the configuration  $d^7$  of  $\text{Co}^{2+}$ , and therefore we shall need to consider both types of normal modes in our discussion.

The departures of the six atoms of the complex span a re-

$Q_j$	$x_1$	$y_1$	$z_1$	$x_2$	$y_2$	$z_2$	$x_3$	$y_3$	$z_3$	$x_4$	$y_4$	$z_4$	$x_5$	$y_5$	$z_5$
$2\sqrt{3}Q_1$	-2	0	0	1	$\sqrt{3}$	0	1	$-\sqrt{3}$	0	0	0	0	0	0	0
$2\sqrt{3}Q_2$	0	2	0	$\sqrt{3}$	-1	0	$-\sqrt{3}$	-1	0	0	0	0	0	0	0
$\sqrt{2}Q_3$	0	0	0	0	0	0	0	0	0	1	0	0	1	0	0
$\sqrt{2}Q_4$	0	0	0	0	0	0	0	0	0	0	1	0	0	1	0
$\sqrt{3}Q_5$	1	0	0	1	0	0	1	0	0	0	0	0	0	0	0
$\sqrt{3}Q_6$	0	1	0	0	1	0	0	1	0	0	0	0	0	0	0
$\sqrt{3}Q_7$	0	0	1	0	0	1	0	0	1	0	0	0	0	0	0
$\sqrt{2}Q_8$	0	0	0	0	0	0	0	0	0	0	0	1	0	0	1
$\sqrt{2}Q_9$	0	0	0	0	0	0	0	0	0	0	-1	0	0	1	0
$\sqrt{2}Q_{10}$	0	0	0	0	0	0	0	0	0	1	0	0	-1	0	0

TABLE XVI: The six even (1-6) and four odd (7-10) normal modes  $E'$  that are relevant to our problem. The numbers are the coefficients of the departures  $\mathbf{u}_j = \{x_j, y_j, z_j\}$  of the  $j$ -th ion from their equilibrium position.

ducible representation  $\Gamma$  of the  $D_{3h}$  group, that can be reduced as follows:  $\Gamma = 2A'_1 + A'_2 + 4E' + 3A''_2 + 2E''$  (see e.g. the Eq. (9.19) in reference [39]). Of these irreducible representations, the  $A'_2$  corresponds to an axial rotation, one  $E'$  to two equatorial rotations, one  $A''_2$  to an axial translation and one  $E'$  to two equatorial translations. After eliminating these three translations and rotations we are left with three even irreducible representations  $E'$ , as well as two  $A''_2$  and one  $E''$  odd representations. The six even normal modes ( $Q_1, \dots, Q_6$ ) transform in pairs like the partners of  $E'$ ; they have been obtained employing standard techniques [39, 40] and are defined in table XVI. In the same way the two modes  $A''_2$  ( $Q_7, Q_8$ ) and the two partners of  $E''$  ( $Q_9, Q_{10}$ ) have been obtained, and are defined in the same table.

The modes  $Q_3, Q_4$ , and  $Q_8$  are translations of only the two axial oxygens, and the  $Q_5, Q_6$ , and  $Q_7$  are translations of only the three equatorial oxygens while  $Q_9$  and  $Q_{10}$  are rotations along the  $x$  and  $y$  axis of the two axial oxygens. As these modes are only partial rotations or translations they are capable of changing the crystal field. The  $x$  and  $y$  rotations of the three equatorial oxygens can be combined with  $Q_9$  and  $Q_{10}$  to give full rotations of the trigonal bipyramid, and the  $z$  rotation of the three equatorial oxygens is already a full rotation, so these three sets of displacements would not appear in our calculation.

From tables XII, XIII, and XIV we can calculate the displacements  $\mathbf{u}_j$  of the five O with respect to their positions in the reference trigonal bipyramid (cf. section IV D 1) and calculate the corresponding normal modes  $Q_j$  defined in table XVI. Employing these  $Q_j$  we calculate in the next two sections the  $g$  values of the distorted complex.

#### 4. The effect of the normal modes on the crystal field

We can now try and find an expression similar to Eq. (5) for the trigonal bipyramid. To this purpose we have employed a relation equivalent to Eq. (20) to calculate, for each of the ten normal modes  $Q_j$  given in table XVI, the change in the crystal field  $V_{cf}(\mathbf{r})$  when all the ligands are displaced from their equilibrium position in the reference complex by a small

$M_L$	$M'_L$	$\langle {}^4F, M_S, M_L   V'_{CF}   {}^4F, M_S, M'_L \rangle$
-3	-2	$-(3c_2 + 10c_4) Q_e^* / (7\sqrt{3})$
-3	-1	$(6c_2 Q_a - 15c_4 Q_b) / (56\sqrt{5})$
-3	0	$\sqrt{15} c_4 Q_d / 4$
-3	1	$-\sqrt{5} c_4 Q_c^* / 16$
-2	-1	$-(9c_2 - 40c_4) Q_e^* / (21\sqrt{5})$
-2	0	$(12c_2 Q_a + 5c_4 Q_b) / (56\sqrt{10})$
-2	1	$\sqrt{5} c_4 Q_d / (2\sqrt{6})$
-2	2	$-5c_4 Q_c^* / (16\sqrt{3})$
-1	0	$-\sqrt{2} (3c_2 - 25c_4) Q_e^* / (35\sqrt{3})$
-1	1	$(18c_2 Q_a + 25c_4 Q_b) / (140\sqrt{3})$
-1	2	$-\sqrt{5} c_4 Q_d / (2\sqrt{6})$
-1	3	$-\sqrt{5} c_4 Q_c^* / 16$
0	1	$\sqrt{2} (3c_2 - 25c_4) Q_e^* / (35\sqrt{3})$
0	2	$(12c_2 Q_a + 5c_4 Q_b) / (56\sqrt{10})$
0	3	$-\sqrt{15} c_4 Q_d / 4$
1	2	$(9c_2 - 40c_4) Q_e^* / (21\sqrt{5})$
1	3	$(6c_2 Q_a - 15c_4 Q_b) / (56\sqrt{5})$
2	3	$(3c_2 + 10c_4) Q_e^* / (7\sqrt{3})$

TABLE XVII: The non-zero matrix elements of the crystal field  $V'_{CF} = \sum_j Q_j V_j(\mathbf{r})$  generated by the normal modes  $Q_1, \dots, Q_{10}$  between states  $|\alpha, S, M_S, L, M_L\rangle = |{}^4F M_S M_L\rangle$  in the subspace  ${}^4F \times {}^4F$ . Only the elements corresponding to the upper triangle of the matrix are given, and the remaining ones are obtained by Hermitian conjugation. The matrix is independent of, and diagonal in, the spin components  $M_S$ . To compress the table we have used the following abbreviations:  $Q_a = (Q_2 + iQ_1) + 5(Q_6 + iQ_5)$ ,  $Q_b = 3(Q_2 + iQ_1) + 7(Q_6 + iQ_5)$ ,  $Q_c = 9(Q_2 + iQ_1) + (Q_6 + iQ_5)$ , (even modes) and  $Q_d = iQ_7$ ,  $Q_e = (iQ_9 + Q_{10})$  (odd modes), as well as their complex conjugates  $Q_a^*$ ,  $Q_b^*$ ,  $Q_c^*$ ,  $Q_d^*$  and  $Q_e^*$ .

$M_L$	$M'_L$	$\langle {}^4P, M_S, M_L   V'_{CF}   {}^4P, M_S, M'_L \rangle$
-1	0	$3c_2 Q_e^* / 5$
-1	1	$-3\sqrt{3} c_2 Q_a / 20$
0	1	$-3c_2 Q_e^* / 5$

TABLE XVIII: Same as in table XVII but for the sub-matrix  ${}^4P \times {}^4P$ . The same abbreviations are used here.

fraction  $\varepsilon$  of that particular normal mode  $Q_j$ . Expanding this change of  $V_{cf}(\mathbf{r})$  in a power series of the coefficient  $\varepsilon$  and taking the linear terms in  $\varepsilon$  gives the corresponding  $V_j(\mathbf{r})$  from Eq. (5). As we are only interested in the subspace  $\{{}^4F, {}^4P\}$  with  $S = 3/2$  of the configuration  $d^7$ , and the  $V_j(\mathbf{r})$  are independent of the spin component  $M_S$ , we need a  $10 \times 10$  matrix  $\langle {}^4L, M_S, M_L | V'_{CF} | {}^4L', M_S, M'_L \rangle$  for each  $Q_j$ , with fixed  $M_S$  and  $L, L' = 3, 1$ . There are regularities between the matrix elements associated to different  $Q_j$ , and we shall employ the following abbreviations:  $Q_a = (Q_2 + iQ_1) + 5(Q_6 + iQ_5)$ ,  $Q_b = 3(Q_2 + iQ_1) + 7(Q_6 + iQ_5)$ ,  $Q_c = 9(Q_2 + iQ_1) + (Q_6 + iQ_5)$ ,  $Q_d = iQ_7$ , and  $Q_e = 9(Q_{10} + iQ_9)$ , as well as their complex conjugates  $Q_a^*$ ,  $Q_b^*$ ,  $Q_c^*$ ,  $Q_d^*$  and  $Q_e^*$ . In tables XVII and XVIII we give the non-zero matrix elements in the upper triangle of the submatrices  ${}^4F \times {}^4F$  and  ${}^4P \times {}^4P$  respectively, and in table XIX we give all those associated with  ${}^4P \times {}^4F$ ; the remaining

$M_L$	$M'_L$	$\langle {}^4P, M_S, M_L   V'_{CF}   {}^4F, M_S, M'_L \rangle$
-1	-3	$(72 c_2 Q_a^* - 5 c_4 Q_b^*) / (56\sqrt{30})$
-1	-2	$\sqrt{2}(12 c_2 + 5 c_4) Q_e / (7\sqrt{15})$
-1	0	$-2(18 c_2 + 25 c_4) Q_e^* / 105$
-1	1	$(24 c_2 Q_a - 25 c_4 Q_b) / (280\sqrt{2})$
-1	2	$\sqrt{5} c_4 Q_d / 4$
-1	3	$-\sqrt{5} c_4 Q_c^* / (8\sqrt{6})$
0	-3	$-\sqrt{5} c_4 Q_d / (4\sqrt{3})$
0	-2	$(12 c_2 Q_a^* + 5 c_4 Q_b^*) / (28\sqrt{10})$
0	-1	$\sqrt{2}(24 c_2 - 25 c_4) Q_e / (35\sqrt{3})$
0	1	$-\sqrt{2}(24 c_2 - 25 c_4) Q_e / (35\sqrt{3})$
0	2	$(12 c_2 Q_a + 5 c_4 Q_b) / (28\sqrt{10})$
0	3	$-\sqrt{5} c_4 Q_d / (4\sqrt{3})$
1	-3	$-\sqrt{5} c_4 Q_c / (8\sqrt{6})$
1	-2	$\sqrt{5} c_4 Q_d / 4$
1	-1	$(24 c_2 Q_a^* - 25 c_4 Q_b^*) / (280\sqrt{2})$
1	0	$2(18 c_2 + 25 c_4) Q_e^* / 105$
1	2	$-\sqrt{2}(12 c_2 + 5 c_4) Q_e / (7\sqrt{15})$
1	3	$(72 c_2 Q_a - 5 c_4 Q_b) / (56\sqrt{30})$

TABLE XIX: Same as in table XVII but for the sub-matrix  ${}^4P \times {}^4F$ . All the non zero matrix elements are given here, and those corresponding to the sub-matrix  ${}^4F \times {}^4P$  are obtained by Hermitian conjugation. The same abbreviations are used here.

non-zero elements are obtained by Hermitian conjugation. It is interesting to note that the matrix elements associated to  $Q_3$ ,  $Q_4$ , and  $Q_8$  are all zero: these modes involve only the two axial ions, and the corresponding two atom partial complex is not only invariant against the operations of  $D_{3h}$ , but also against a twofold axis along the  $z$  direction. This extra symmetry forces all the one-electron matrix elements between  $d$  states of the crystal field associated to  $Q_3$ ,  $Q_4$ , and  $Q_8$  to be zero.

As in the crystal field of the reference complex, the  $V'_{CF}$  has coefficients containing the Co-O distances  $R_a$  and  $R_c$ , as well as the atomic averages  $\langle r^2 \rangle$  and  $\langle r^4 \rangle$ , and they appear as  $c_2$  and  $c_4$  in the tables XVII, XVIII and XIX. As the  $R_a$  and  $R_c$  are nearly the same, it is possible from Eq. (19) to relate the crystal field parameters  $D_s$  and  $D_t$  to these two coefficients. Assuming that  $R_a = R_c$  we obtain  $c_2 = 14 D_s$  and  $c_4 = (168/25) D_t$ , but we have derived slightly better relations considering the difference between  $R_a$  and  $R_c$ :

$$c_2 = \frac{7}{-(3/2) + 2 (R_a/R_c)^3} D_s, \quad (21)$$

$$c_4 = \frac{21}{(9/8) + 2 (R_a/R_c)^5} D_t.$$

As with the reference complex, we employ the 3-j coefficients to calculate the matrix elements of the crystal field  $V'_{CF}$  in the representation that diagonalizes the total  $J$  and  $J_z$ , because the doublets  $|d^7 \alpha SLJM_J\rangle$  are basis for the irreducible representations of the reference trigonal bipyramid, and the eigenstates of the reference complex would then belong to subspaces with fixed  $M_J$ . In section IVD 2 we have shown

	$g_1$	$g_2$	$g_3$	$g_{av}$
PO <sub>4</sub>				
$b_0$	4.8027	4.8027	1.9904	3.8653
$b_1$	5.0477	4.5577	2.2998	3.9684
$b_2$	5.0477	4.5577	1.9904	3.8653
$c_0$	5.0435	5.0435	1.9829	4.0233
$c_1$	5.7379	4.3492	2.1171	4.0680
$c_2$	5.7379	4.3492	1.9829	4.0233
AsO <sub>4</sub>				
$b_0$	4.8723	4.8723	1.9885	3.9110
$b_1$	5.7637	4.2279	2.2364	4.0760
$b_2$	5.7637	4.2279	1.9885	3.9934
$b_3$	5.6402	4.1044	1.9885	3.9110
$c_0$	5.0667	5.0667	1.9818	4.0384
$c_1$	7.1232	3.5385	1.9854	4.2157
$c_2$	7.1232	3.5385	1.9818	4.2145
$c_3$	6.8591	3.2744	1.9818	4.0384

TABLE XX: The principal components of the calculated  $\mathbf{g}$  tensor for the penta-coordinated  $\text{Co}^{2+}$  and their average  $g_{av}$  in  $\text{Co:Zn}_2(\text{OH})\text{PO}_4$  and  $\text{Co:Mg}_2(\text{OH})\text{AsO}_4$ . The rows  $b_0$  and  $c_0$  are for the reference trigonal bipyramid, while  $b_1$ ,  $b_2$ ,  $b_3$ ,  $c_1$ ,  $c_2$ , and  $c_3$  include the effect of deformations produced by the crystallographically calculated normal modes. Rows  $b_1$  and  $c_1$  include all the normal modes, while  $b_2$  and  $c_2$  only include the even modes, and in rows  $b_3$  and  $c_e$  we have also put  $Q_1 = Q_2 = 0$ . The values of  $B$ ,  $D_s$ ,  $D_t$  and  $\zeta$  employed here for rows  $b_j$  ( $j = 0 - 3$ ) are given in row b of table XV, and those corresponding to rows  $c_j$  are given in row c of that table.

that, with the two sets of parameters  $B$ ,  $D_s$  and  $D_t$  obtained in that section, the two lowest doublets belong to the  $M_J = 1/2$  and  $M_J = 3/2$  subspaces and that they are separated by more than  $75 \text{ cm}^{-1}$ , while the remaining doublets are more than  $2300 \text{ cm}^{-1}$  above them. A good approximation to calculate the effect of  $V'_{CF}$  on these levels is then to consider the total Hamiltonian inside the two subspaces  $M_J = 1/2, 3/2$ , and one has then to consider a matrix of  $26 \times 26$  elements, corresponding to values of  $J$  equal to  $9/2, \dots, 1/2$ . The eigenstates of this matrix show that there is no change in the relative position of the two lowest doublets, so that the ground state remains  $M_J = 1/2$ .

### 5. The g-factors of the penta-coordinated $\text{Co}^{2+}$ .

To calculate the spin Hamiltonian we employ the traditional method [41]. In the present case we consider the four states of the two lowest doublets of the reference trigonal bipyramid calculated in section IVD 2 as the eigenstates of the unperturbed Hamiltonian, with  $M_J = 1/2$  as the ground doublet and  $M_J = 3/2$  as the excited one. Both the Zeeman term and the crystal field  $V'_{CF}$  produced by the deformation of the normal modes are the perturbations, and in the usual way we find the gyromagnetic tensor  $\mathbf{g}$  in second order. We have calculated the three components of  $\mathbf{g}$  for the penta-coordinated  $\text{Co}^{2+}$  for all the sets of  $B$ ,  $D_s$  and  $D_t$  given in table XV, and the results are given in table XX. The values corresponding to the reference trigonal bipyramid are given in the rows  $b_0$  and  $c_0$ , while those given in the rows  $b_j$  and  $c_j$  (with  $j = 1, 2$  for the phosphate

and  $j = 1, 2, 3$  for the arsenate) have been calculated employing the normal modes  $Q_j$  derived from the crystallographic positions (cf. table XII) as discussed in section IV D 3. One verifies in table XX that the average of the principal values of  $\mathbf{g}$  is not very different from 4.33, but that it changes with  $B$  and the crystal field parameters more than in the octahedral case. The rows  $b_1$  and  $c_1$  include the effect of all normal modes, while in  $b_2$  and  $c_2$  only the even modes are considered. In the phosphate case, the crystallographic  $Q_1 = Q_5 = 0$ , and for the arsenate we have also imposed this condition in rows  $b_3$  and  $c_3$ . From table XX we conclude that

- With only even modes and  $Q_1 = Q_5 = 0$  (compare rows  $b_2$  and  $c_2$  in phosphate and  $b_3$  and  $c_3$  in arsenate with rows  $b_1$  and  $c_1$ ) the average  $g$  is not altered by the lower symmetry crystal fields generated by the remaining normal modes, and these fields affect the equatorial components of  $\mathbf{g}$ , but leave their sum and the axial component unaffected.
- Only the axial  $g$ -factor is altered by the inclusion of the odd modes, while the two equatorial  $g$ -factors are not altered (compare rows  $b_1$  with  $b_2$  and  $c_1$  with  $c_2$ ). This result is true both with  $Q_1 = Q_5 = 0$  (in the phosphate) or otherwise (in the arsenate).
- The fields associated to the modes  $Q_1$  and  $Q_5$  change the sum of the two equatorial  $g$ -factors but leave the axial value unaffected (compare rows  $b_2$  with  $b_3$  and  $c_2$  with  $c_3$  in the arsenate).

From the calculations in the present section, it follows that one should observe an allowed ESR line of  $\text{Co}^{2+}$  from the penta-coordinated complex when that site is occupied. We have seen in Section IV B that besides the lines associated to the octahedral spectra, there are some weak extra lines that could be interpreted as belonging to that complex: their estimated  $g$ -factors are given in rows b) of table VIII, and should be compared with the values given in table XX, that were calculated for different sets of parameters derived from the optical spectra and with normal modes calculated from the crystallographic positions. It is clear that the arsenate values in row  $c_3$  of table XX are fairly close to the estimated values in row  $b$  from table VIII. It is well known that the  $g(i)$  obtained from the crystallographically calculated normal modes are generally different from those experimentally observed, as discussed for the octahedral compounds (cf. section IV C), and we could expect that a good fitting could be obtained by making small changes in the crystallographic normal modes. To verify this assumption it is sufficient to change only  $Q_2$  and  $Q_6$ , keeping all the remaining modes at their crystallographic values. Employing  $Q_2/R_a = -0.03$  and  $Q_6/R_a = -0.07$  for the phosphate we find  $g(1) = 7.05$ ,  $g(2) = 3.03$ , and  $g(3) = 2.12$ , while for the arsenate we obtain  $g(1) = 7.62$ ,  $g(2) = 3.04$ , and  $g(3) = 1.99$  with  $Q_2/R_a = 0.01$  and  $Q_6/R_a = -0.07$ . These fittings are fairly good, and show that the ESR spectra of  $\text{Co}^{2+}$  in the two compounds can be described perfectly well within our theory, but the crystal fields obtained can not be taken too seriously because of the very large errors in the experimental  $\mathbf{g}$  tensor.

We notice that the relative intensities of the extra lines in Fig. 4 are rather smaller than those in Fig. 5. This can be understood because the concentration of  $\text{Co}^{2+}$  in the arsenate is ten times larger than in the phosphate, and this should also alter their relative occupations.

The rather small intensity of the lines that could be attributed to the penta-coordinated complex indicates a very small occupation of  $\text{Co}^{2+}$  in the penta-coordinated sites. This conjecture has been verified [3], from the heat of formation of these compounds, estimated by a molecular orbital calculation of the heats of formation of the clusters  $[\text{M}(\text{OP}(\text{OH})_3)_n]^{2+}$ ,  $n = 5, 6$  and  $\text{M} = \text{Co}$  and  $\text{Zn}$ .

## V. CONCLUSIONS

We have discussed the ESR of the ion  $\text{Co}^{2+}$  in different systems:  $\text{Co}^{2+}$  in a  $\text{MgO}$  crystal [1],  $\text{Co}^{2+}$  in single crystal and powder samples of  $\text{NH}_4\text{NiPO}_4 \cdot 6\text{H}_2\text{O}$  [2] and  $\text{Co}^{2+}$  in powders of  $\text{Co}_2(\text{OH})\text{PO}_4$  and  $\text{Co}_2(\text{OH})\text{AsO}_4$  [3].

The  $\text{Co}^{2+}$  in a  $\text{MgO}$  crystal is in an octahedral symmetry, and we discuss why it retains its cubic symmetry although it would be naively expected to suffer a static Jahn-Teller deformation, because the ground term  ${}^4F$  has a rather large orbital degeneracy. We then briefly discuss the origin of this effect, and point out how the Jahn-Teller crystal fields affect the properties of the system, like the ESR and the electronic Raman scattering from  $\text{Co}^{2+}$ .

When  $\text{Co}^{2+}$  substitutes  $\text{Ni}^{2+}$  in single crystals of  $\text{NH}_4\text{NiPO}_4 \cdot 6\text{H}_2\text{O}$  its nearest O form a deformed octahedron, and we study the effect of the non-cubic crystal fields employing the normal modes of the octahedron to simplify the systematic study of the effect of these fields.

There are two type of sites of  $\text{Co}^{2+}$  in the compounds  $\text{Co}_2(\text{OH})\text{PO}_4$  and  $\text{Co}_2(\text{OH})\text{AsO}_4$  of the adamite type: a deformed octahedron and a deformed trigonal bipyramid, and we have analyzed the ESR of impurities of  $\text{Co}^{2+}$  in synthetic crystals of  $\text{Zn}_2(\text{OH})\text{PO}_4$ ,  $\text{Mg}_2(\text{OH})\text{AsO}_4$  in powder form. Crystal field theory has been employed to try and understand the experimental ESR results for the two  $\text{Co}^{2+}$  complexes with coordination five and six that are present in the adamite structure. The Racah parameter  $B$  as well as the crystal fields  $D_q$  for the octahedral complex and both  $D_s$  and  $D_t$  for the trigonal bipyramid one have been estimated from the assignments that were made of the diffuse reflectance spectrum of these two complexes. Two alternative sets of parameters were proposed for the penta-coordinated complex.

From the crystallographic structure, a reference octahedron centered in the  $\text{Co}^{2+}$  was defined, such that the normal modes of the complex corresponding to rotations and expansions would be zero and the remaining normal modes would not have any contribution of these irrelevant deformations, and following the same method employed to study the ESR of  $\text{Co}^{2+}$  in  $\text{NH}_4\text{NiPO}_4 \cdot 6\text{H}_2\text{O}$ , the crystal fields that would reproduce the experimental  $\mathbf{g}$  tensor of the octahedral complex in both  $\text{Zn}_2(\text{OH})\text{PO}_4$  and  $\text{Mg}_2(\text{OH})\text{AsO}_4$  have been obtained..

As the penta-coordinated complex seems to have at most minor contributions to the ESR spectra, we have analyzed the

possible motives for this behavior. We argue that two doublets with  $M_J = \pm 1/2$  and  $M_J = \pm 3/2$  would be lowest in energy, separated by a rather large excitation energy from the remaining excited states. The  $M_J = \pm 3/2$  has forbidden ESR transitions, and this would explain the experimental results if that were the ground doublet, but when the crystal field of the trigonal bipyramid is considered together with the spin-orbit interaction, it was found that the  $M_J = \pm 1/2$  doublet, with allowed ESR transitions, is the lowest. To verify whether this result would be altered by the deformations of the trigonal bipyramid, we considered their effects in a way similar to that employed in the octahedral case to calculate the  $\mathbf{g}$  tensor. First it was necessary to derive the normal modes of the trigonal bipyramid that are relevant to our problem, and they are given in table XVI. The corresponding Jahn-Teller contributions  $V'_{CF}$  to the crystal field, whose non-zero matrix elements  $\langle {}^4L, M_S, M_L | V'_{CF} | {}^4L', M_S, M'_L \rangle$ , for  $L, L' = 3, 1$ , are given in tables XVII, XIX and XVIII. Defining a reference perfect trigonal bipyramid by the same method employed in the octahedral case, the values of the relevant normal modes were obtained by employing the crystallographic positions, and subsequently used to calculate their effect on the relative position of the two lowest doublets. No appreciable change was found, and as an alternative explanation we assumed that the penta-coordinated complex is scarcely occupied in the dilute system. This conclusion is compatible with the calculation of the heat of formation of the octahedral and the trigonal bipyramid complexes with both Co and Zn as the central ions, calculated in reference [3].

Employing the Jahn-Teller crystal fields together with the normal modes calculated from the crystallographic distortions, it was possible to calculate the  $\mathbf{g}$  tensor, shown in ta-

ble XX for both the perfect and deformed trigonal bipyramid, this last subjected to different deformations. The trace of the  $\mathbf{g}$  tensor in the perfect trigonal bipyramid changes more with the parameters  $B, D_s$  and  $D_t$  than in the octahedral case, where it is always fairly close to 13.

The trigonal bipyramid has no center of symmetry, and it was necessary to consider all the normal modes, even those that are odd against reflection in the horizontal symmetry plane. We have shown that these last modes affect the axial component of  $\mathbf{g}$  but that they have little or no effect on the two equatorial components. The experimental  $\mathbf{g}$ -tensor of the penta-coordinated complex could be measured but with rather large errors. As in the octahedral case, the crystallographically determined normal modes could not explain the observed values, but for the two type of complexes it was possible to find values of the normal modes that would generate crystal fields that describe the experimental ESR spectra for both the phosphate and arsenate compounds.

We conclude that both our theoretical analysis of the ESR of the systems studied, as well as the molecular orbital calculation of the formation energies, coincide in assigning a rather small relative occupation of the penta-coordinated sites with respect to the octahedral ones in those systems. The experimental spectra of both the octahedral and penta-coordinated complexes can be understood by considering the effect of the crystal fields generated by the corresponding normal modes on the  $\mathbf{g}$  tensor.

## Acknowledgments

The authors would like to acknowledge financial support from the following agencies: FAPESP and CNPq.

- 
- [1] L. T. Peixoto and M. E. Foglio, *Revista Brasileira de Física* **13**, 564 (1983).
  - [2] A. Goñi, L. M. Lezama, T. Rojo, M. E. Foglio, J. A. Valdivia, and G. E. Barberis, *Phys. Rev. B* **57**, 246 (1998).
  - [3] M. E. Foglio, M. C dos Santos, G. E. Barberis, J. M. Rojo, J. L. Mesa, L. Lezama, and T. Rojo, *J. Phys.: Condens. Matter* **14**, 2025 (2002).
  - [4] J. H. Van Vleck, *J. Chem. Phys.* **7**, 72 (1939).
  - [5] The definitions of the normal coordinates  $Q_j$  we employ in this work are slightly different from those in reference 4.
  - [6] G. F. Koster, J. O. Dimmock, R. G. Wheeler, and H. Stats, *Properties of the thirty-two point groups* (M.I.T. Press, Cambridge, Massachusetts, 1963).
  - [7] H. A. Jahn, *Proc. Roy. Soc. A* **164**, 117 (1937).
  - [8] H. A. Jahn, E. Teller *Proc. Roy. Soc. A* **161**, 220 (1937).
  - [9] A. Abragam and B. Bleaney, *EPR of Transition Ions* (Clarendon Press, Oxford, 1970).
  - [10] M. Tinkham, *Proc. Roy. Soc. (London) A*, **236**, 549 (1956).
  - [11] E. B. Tucker, *Phys. Rev.* **143**, 264 (1966).
  - [12] F. S. Ham, W. M. Schwarz, and M. O'Brien *Phys. Rev.* **185**, 548 (1969).
  - [13] T. Ray and J. R. Regnard, *Phys. Rev. B* **9**, 2110 (1974).
  - [14] W. Low, *Phys. Rev.* **109**, 256 (1958).
  - [15] G. Peckham, *Proc. Phys. Soc. London* **90**, 657 (1967).
  - [16] S. Guha, *Phys. Rev. B* **21**, 5808 (1980).
  - [17] C. H. P. Poole and H. A. Farach, *The Theory of Magnetic Resonance* (Wiley, New York, 1972).
  - [18] A. Goñi, J. L. Pizarro, L. M. Lezama, G. E. Barberis, M. I. Arriortua, and T. Rojo, *J. Mater. Chem.* **6**, 412 (1996).
  - [19] A. Abragam and M. H. L. Pryce, *Proc. Roy. Soc. (London) A*, **206**, 173 (1951).
  - [20] L. T. Peixoto and M. E. Foglio, *Revista Brasileira de Física* **13**, 564 (1983).
  - [21] M. E. Foglio *Ph.D. Thesis* (University of Bristol, Bristol, England, 1962).
  - [22] F. C. Hawthorne, *Can. Mineral.* **14**, 143 (1976).
  - [23] R. J. Hill, *Am. Mineral.* **61**, 979 (1976).
  - [24] W. T. A. Harrison, J. T. Vaughey, L. L. Dussack, A. J. Jacobson, T. E. Martin, and G. D. Stucky, *J. Solid State Chem.* **114**, 151 (1995).
  - [25] P. Keller, *Neues Jahrb. Mineral. Monatsh.* 560 (1971).
  - [26] P. Keller, H. Hess, and F. Zettler, *Neues Jahrb. Miner. Abh.* **134**, 147 (1979).
  - [27] H. Riffel, F. Zettler, and H. Hess, *Neus Jahrb. Mineral. Monatsch.* 514 (1975).
  - [28] J. M. Rojo, *Ph. D thesis*, Universidad del Pais Vasco, Bilbao, 2000.
  - [29] A. Abragam and B. Bleaney, *Electron Paramagnetic Resonance*

- of Transition Ions* (Clarendon Press, Oxford, 1970). See pag. 449.
- [30] F. G. Beltran and F. Palacio, J. Phys. Chem. **80**, 1373 (1976).
  - [31] F. Palacio, J. Phys. Chem. **82**, 825 (1978).
  - [32] J. M. Rojo, J. L. Mesa, L. Lezama, G. E. Barberis, and T. Rojo, J. Magn. Magn. Mat. **157/158**, 493 (1996).
  - [33] M. M. Rojo, J. L. Mesa, J. L. Pizarro, L. Lezama, M. I. Arriortua, and T. Rojo, J. Solid State Chem. **132**, 107 (1997).
  - [34] When we derive the system parameters of the octahedral complexes from the optical spectra, we have shifted the ground orbital level by the spin orbit correction, estimated to be  $2.5 \alpha \lambda \sim -635 \text{ cm}^{-1}$ . This improvement was not used in the penta-coordinated complex.
  - [35] J. S. Wood, Inorg. Chem. **7**, 852 (1968).
  - [36] J. S. Griffith, *The theory of transition-metal ions*. (University Press, Cambridge, England, 1961), see Eq. (6.37).
  - [37] U. Fano and G. Racah, *Irreducible tensorial sets*. (Academic Press, New York, 1959).
  - [38] C. W. Nielsen and G. F. Koster, *Spectroscopic coefficients for the  $p^n$ ,  $d^n$ , and  $f^n$  configurations*. (MIT Press, Boston, Mass. 1963).
  - [39] L. A. Woodward, *Introduction to the theory of molecular vibrations and vibration spectroscopy*. (Clarendon Press, Oxford, 1972).
  - [40] E. B. Wilson, J. C. Decius, and P. C. Cross, *Molecular vibrations*. (McGraw-Hill, New York, 1955).
  - [41] H. M. L. Pryce, Proc. Roy. Soc.(London) A, **63**, 25 (1950).